SAND2017-5609C

AlN and ScAlN Contour Mode Resonators for RF Filters

M.D. Henry, R.P. Timon, T.R. Young, C.D. Nordquist, B.A. Griffin

Sandia National Laboratories, Albuquerque, NM, 87185, USA

Piezoelectric acoustic resonators are widely utilized for RF devices but most can only utilize a few different resonant frequencies on the same substrate. Contour mode resonators (CMR) have resonant frequencies defined lithographically offering the advantage of an extensive frequency range on the same film, wafer, or die. This work will discuss our efforts in developing ScAlN for CMRs to achieve RF performance suitable for use in RF filters. First we will discuss our RF sputter deposition process for creating high-performance $Sc_{0.12}Al_{0.88}N$ piezoelectric films and compare it with an established sputtered piezoelectric AlN. Fabrication and integration techniques for fabricating CMRs will be then detailed. Finally, electrical design and resonator performance is then discussed. These early investigations into ScAlN films suggest that performance metrics such as k^2_{eff} can substantially improve while simultaneously ensuring good resonator Q factors over a wide frequency range of devices.

Introduction

A strong technological pull for piezoelectric microelectromechanical system (MEMS) resonators exists from radio frequency (RF) filters in telecommunication devices such as cell phones and personal tablets[1]. The majority of the filters utilize architectures such as surface acoustic wave (SAW) or bulk acoustic wave (BAW) resonators due to their manufacturability and RF performance sufficient for telecommunications[2, 3]. However, new designs of contour mode resonators (CMR) have demonstrated the advantage of having a wide frequency range of devices on the same chip because the resonance is acoustically defined by the sidewalls of the device. This feature of CMRs is fundamentally different than BAWs where frequency is set by film thickness [4-6]. CMRs have been fabricated and packaged to demonstrate different frequency RF bandpass filters on the same chip[6, 7]. Every integration step to achieve these suspended acoustic devices, including lithographic patterning and plasma etching, is CMOS compatible and has been demonstrated in back end of the line (BEOL) integrations[8]. A tradeoff with using CMR devices over BAW or SAW is that the electric field induced film strain occurs along a different axis than the field which generates it; the piezoelectric strain matrix coefficient d_{31} would utilize a vertical (i.e., 3) electric field to create strain within the plane of the film (i.e., 1)[9]. In contrast, the d_{33} coefficient correlates the vertical strain generated by a parallel electric field and is generally larger than d_{31}. For AlN, high quality film values for d_{31} are approximately -2.7 pC/N whereas the higher valued d_{33} coupling coefficients are 5.5 pC/N[10]. To understand how the piezoelectric strain coefficient relates to resonator device performance, the coupling coefficient (k^2_t) is used which describes how the electric field transduces an acoustic wave, Eqn 1.

$$k_t^2 = \frac{d_{31}^2 E}{\epsilon} = \frac{\pi^2}{8} \frac{k_{eff}^2}{1-k_{eff}^2} \quad (1)$$

Here, E is the Young's modulus of the piezoelectric film and ∈ is the dielectric permittivity. Defining an effective coupling coefficient (k^2_{eff}) is useful for resonators since it can be measured from electrical performance. The lower valued d_{31} coupling in CMRs directly impacts resonator, and hence RF filter, electrical performance in values such as rejection ratio, filter bandwidth, and insertion loss resulting in high power usage. To utilize the advantages of CMRs such as multiple frequency and ease of integration, improvements in the coupling coefficient of roughly 3 times its current value are needed.

Increasing the effective coupling coefficient of AlN has been predicted and observed when aluminum becomes substituted by scandium in the wurtzite matrix[11, 12]. Due to the reduction of electronegativity from the Sc substitution, the AlN wurtzite matrix become frustrated with increased ionic displacements in a given electric field. Piezoelectric strain matrix d_{33} is suggested to increase from 5.6 pC/N in AlN to beyond 25 pC/N in $Sc_{0.4}Al_{0.6}N$[10, 11]. Although the Young's modulus is expected to also decrease with increasing Sc substitution, substantial increases in k^2_{eff} are still predicted, suggesting that continuing the technological investment in film development for CMRs is warranted.

This work describes the results of optimization of RF sputtered $Sc_{0.12}Al_{0.88}N$ film development from a single ScAl target for width extensional (WE) CMR for RF filter applications. Sputtered films were optimized to remove grain inclusions while maintain as suitable film stress for manufacturing. The results of these films will be discussed and compared with sputtered AlN films deposited in the same tool. This work will then describe fabrication of top electrode WE CMR and discuss major differences in the fabrication of such devices such as etch rates and photoresist developer attack. Comparison of device performance between the ScAlN films and AlN films will then be discussed.

Sputter Deposition of AlN and ScAlN Films

A significant amount of AlN film development and characterization has been published regarding RF reactive sputter deposition of AlN films using both single and co-sputtered targets[10, 13]. Creation of high piezoelectric AlN (0002) films requires control of the deposition as well as the substrate surface on which the polycrystalline film is grown. Alignment of the c-axis has been observed to be dependent on film stress, deposition surface and crystallinity, interface oxidation, and temperature. Ideally AlN films for resonators require growth upon a well textured base metal such as Pt, Al, or Mo for use as a bottom resonator electrode. Quantification of film quality can be difficult with the most precise measurements made by device fabrication. However, close correlation between the x-ray diffraction (XRD) 2-theta scans and rocking curves to piezoelectric properties allows for a cheaper and faster measurement of films. Typically, for k^2_{eff} values to be reasonable for quality devices, rocking curves should have full width half maximum (FWHM) values below 2-3 degrees. Other film properties such as Young's modulus, film stress, and density are also important to measure since they impact many device parameters.

Growth on silicon (100) is considerably easier and less expensive to develop due to the smooth, high quality crystalline surface and minimum surface development and preparation; in this work we use both high (>5kΩ-cm) and low (2-20 Ω-cm) resistivity (100) 6" silicon wafers as the growth surface for AlN and ScAlN films. No native oxide removal or cleans were performed prior to deposition nor was any insitu RF sputter clean utilized. Deposition of both AlN and ScAlN films were performed using a Trikon Sigma

200 physical vapor deposition tool. For the AlN films a 13" high purity Al target was used and for the ScAlN, a casted $Sc_{12.5}Al_{87.5}$ by weight 13" target from Materion was utilized.

AlN was first demonstrated on the tool using 5 KW DC power, 82 KW RF power, Ar flow 25 sccm, N_2 flow of 125 sccm (for a Ar:N_2 ratio of 1:5), and platen temperature of 350 C for approximately 700 nm thick films. XRD shows that the film was significantly c-axis oriented along the (002) orientation at a 2θ angle of 36.082° and a rocking curve FWHM of 2.248°, Fig 1. SEMs confirm a consistent grain structure, Fig 2.

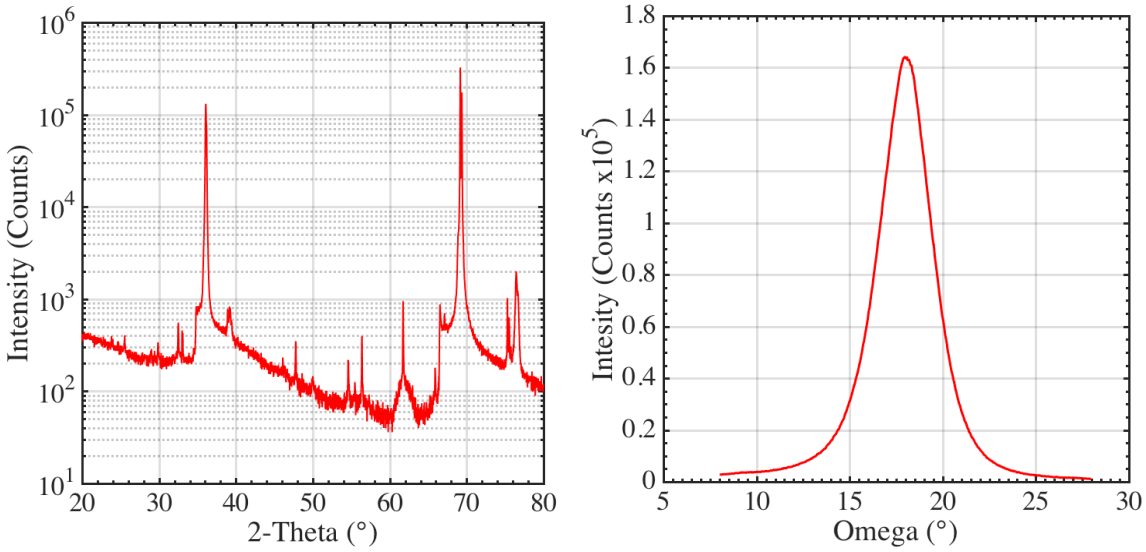

Figure 1. XRD scans of AlN film with a (002) peak located at 36.082° and a rocking curve FWHM of 2.248°.

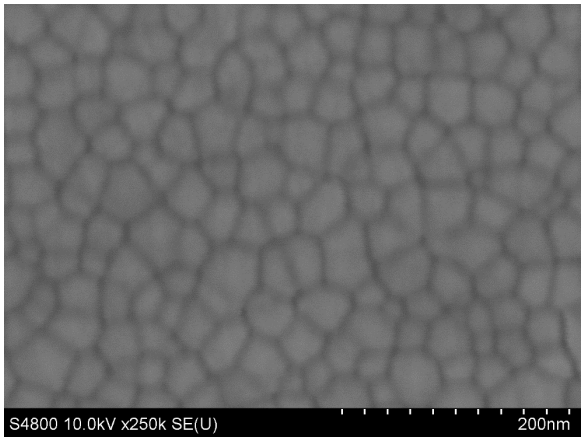

Figure 2. Scanning electron micrograph of AlN film imaging down the c-axis.

The Al target was then removed from the tool and replaced with the ScAl target described earlier. The conditions, noted above, which yielded the good AlN were utilized to deposit the ScAlN. Initial results suggested a very good film with XRD indicating that the film was mostly c-axis oriented at the center of the wafer along the (002) orientation at a 2θ angle of 35.911° with a rocking curve FWHM of 1.906°, Fig 3. Although not displayed, measurements at the wafer edge yielded a 2θ angle of 35.897° and a rocking curve FWHM of 1.917° suggesting good film uniformity. Film thickness and stress were measured at 740 nm and -58 MPa respectively. However, SEM measurement revealed inclusions in the film, Fig 4 a and b. Upon inspection, these inclusions appear to have similar grain structure as the majority of the film but misoriented. In an approximately 20

μm^2 area, 17 of these inclusions are observed. Previous work in AlN has seen structures similar to these when exposed to oxygen, during an increase in Sc content or when growth was interrupted and restarted with reversed grain polarity,[13, 14]. In the case of Sc addition, oxygen incorporation is also suspect due to Sc affinity to O[15]. Although the nature of these inclusions is still unknown, we speculate that the incorporation of Sc is likely involved in creating a new grain structure not oriented around a common axis so they do not show up in XRD.

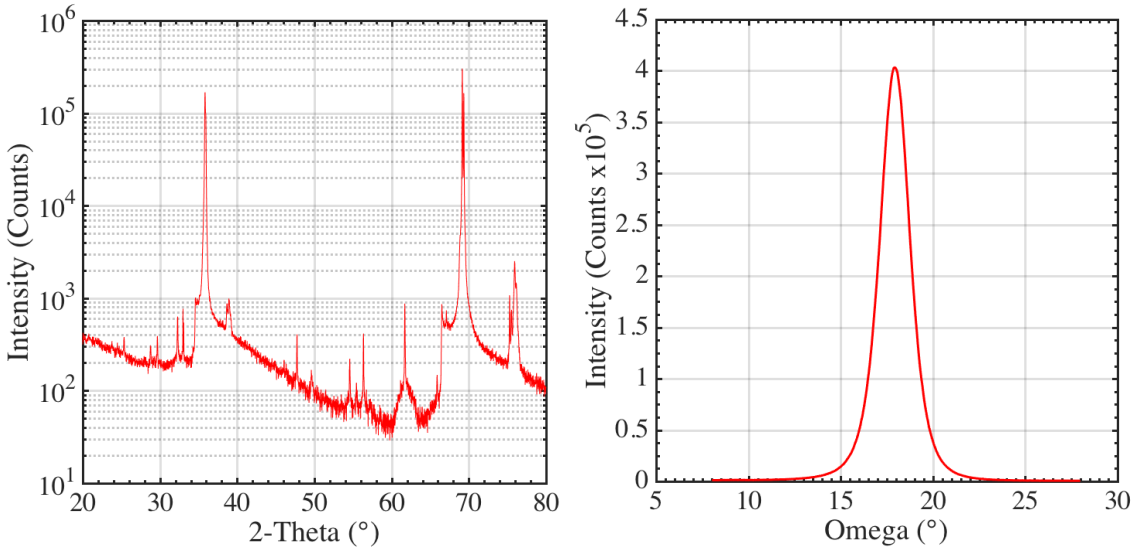

Figure 3. XRD scans of ScAlN film with a (002) peak located at 35.911° and a rocking curve FWHM of 1.906°.

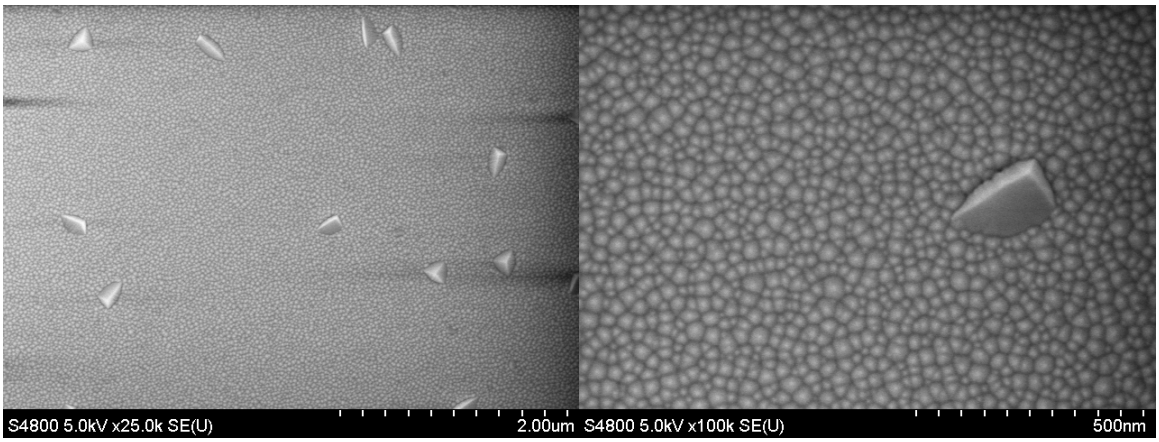

Figure 4. a) Scanning electron micrograph of ScAlN film imaging down the c-axis and demonstrating triangular inclusions in the film. b) Increasing the magnification of the film at the center shows the inclusion with similar grain structure as the film but rotated.

SEM measurements under a magnification of 100k and 50k which images 1.13 μm^2 and 4.54 μm^2 area respectively, of a series of ScAlN films deposited under the exact same conditions sequentially, demonstrated that running a series of dummy wafers before deposition on wafers of interest, baffle wafers, would greatly reduce the number of inclusions, Fig 5. This experiment does lend data to the idea that a chamber or wafer contaminant, such as oxygen or water vapor, could be inducing these inclusions. Since the

baffle wafers are not utilized to generate inclusion free AlN it also suggests that Sc is also a prerequisite for this phenomenon.

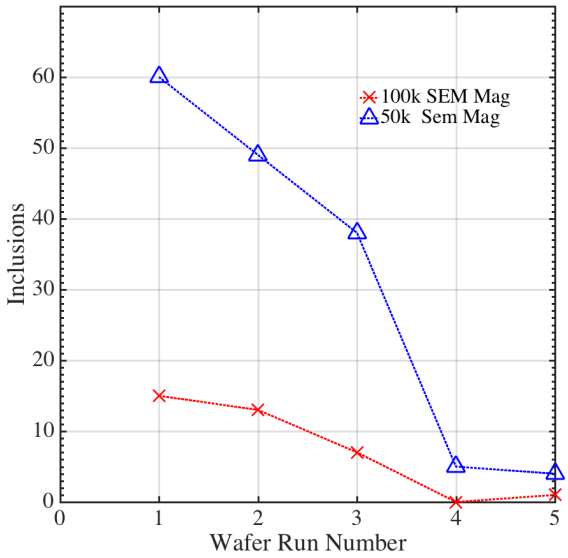

Figure 5. Effect of deposition on baffle wafers prior to depositing on product wafers to reduce the number of inclusions on the wafer as measured in a SEM of 50k ('^') and 100k ('x') magnification.

Fabrication of AlN and ScAlN Resonators

Utilizing the good AlN and ScAlN film deposition processes for 750 nm films, WE CMRs were fabricated. First Al was electron beam evaporated onto the surface of the films. Lithographic patterning of the top electrodes was achieved using UltraI 0.8 photoresist on an antireflection coating and I-patterning using an ASML stepper. The pattern was etched into the Al film using a PlasmaTherm Unaxis inductively coupled plasma reactive ion etcher (ICP RIE). Etch conditions were ICP at 1000 W, bias power at 20 W, BCl_3 and Cl_2 gas at 30 and 12 sccm respectively, at 1.7 mTorr. Under these conditions, when the etch front clears all the unpatterned Al, no discernable AlN or ScAlN is etched. The resist is then stripped and repatterned on the stepper using AZ 4330 photoresist. Wafers are again etched thru the AlN and ScAlN films down to the Si substrate in the ICP RIE under the same conditions but bias power was increased to 200 W. This etch defines the sides of the resonators and hence the resonant frequency. Cross sectional SEM images of test AlN and ScAlN wafers indicate reasonable sidewall profiles and an aligned c-axis grain structure, Fig 6 a and b respectively.

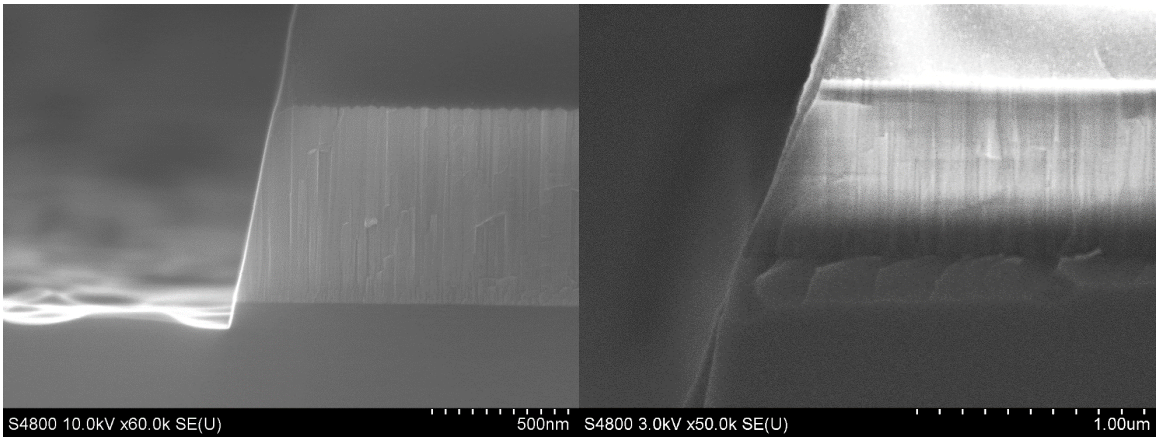

Figure 6. Cross sectional scanning electron micrograph of a) AlN film on Si and b) ScAlN film on Si after etching. Resist was left on the surface of the film and some etching into the Si occurred.

Upon completion of the etch, a controlled isotropic etch of the silicon substrate was performed to suspend the resonator device utilizing Xactix vapor release XeF_2, Fig 7.

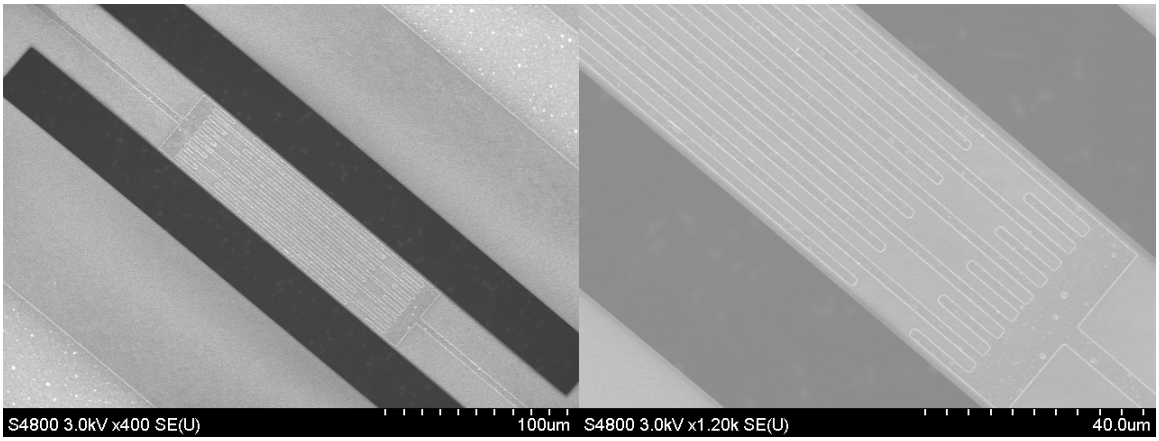

Figure 7. Scanning electron micrograph of released ScAlN WE CMR.

Design and Performance of AlN and ScAlN Resonators

Resonators were designed using 10 interdigitated transducer (IDT) electrodes[16, 17]. The fundamental symmetric (S0) mode was calculated by assuming an acoustic velocity of 10,300 m/sec and each electrode was λ/4 wide with a pitch of λ/2, Eqn 2.

$$f = \frac{v_a}{\lambda} = \frac{1}{W/N_e}\sqrt{\frac{E}{\rho}} \quad (2)$$

Here f is the S0 fundamental frequency, v_a is acoustic velocity, N_e is number of electrode pairs, ρ is the density of the film, W is the resonator width, and λ is the acoustic wavelength. Utilizing 10 electrodes and an electrode offset λ/8 from the etched edge, the width of the resonator is determined by the number of electrode pairs times the designed wavelength, Fig 7b. The aperture (L), the length overlap between opposite electrodes, was designed such that the overlap length to wavelength ratio was held constant at 12. Electrode stubs

and spaces of ¾ λ from the electrical bus bar were utilized to reduce longitudinal spurious modes.

Electrical 2-port testing was performed on released devices using a Keysight RF network analyzer using a two probe GSG (ground signal ground) thru measurement configuration S_{12}. The substrate was left floating such that the Butterworth-Van Dyke (BVD) electrical model was applicable[1, 9]. For both the AlN and ScAlN high resistivity wafers, resonators were tested and Fig 8a displays the S_{12} parameter for each 1601-point narrow range frequency sweep. For comparison a wide range sweep of a ScAlN resonator was performed as was the effect of placing probes on contact pads without a resonator attached, Fig 8b. The wide range sweep measures the off resonance is dominated by the electrode to electrode shunt capacitance. Measurement of the open demonstrates that little of the signal is shunted through the contact pads and substrate. For the 500 to 1500 MHz range displayed, the capacitive insertion loss was approximately -38 to -34 dB. The top of the series resonance, the insertion loss, improved as frequency increased but a general improvement of ScAlN (red) over AlN (blue) is also seen. Further, the ScAlN frequency for a given electrode width, is slightly downshifted due to both a softening of the elastic modulus and increase in density. Since the fabrication was identical for both the wafers, we attribute this improvement directly to piezoelectric strain matrix coefficients. Around 1200 MHz, a double resonance is observed and is attributed to a higher order antisymmetric mode (AS) coupling to the S0 mode.

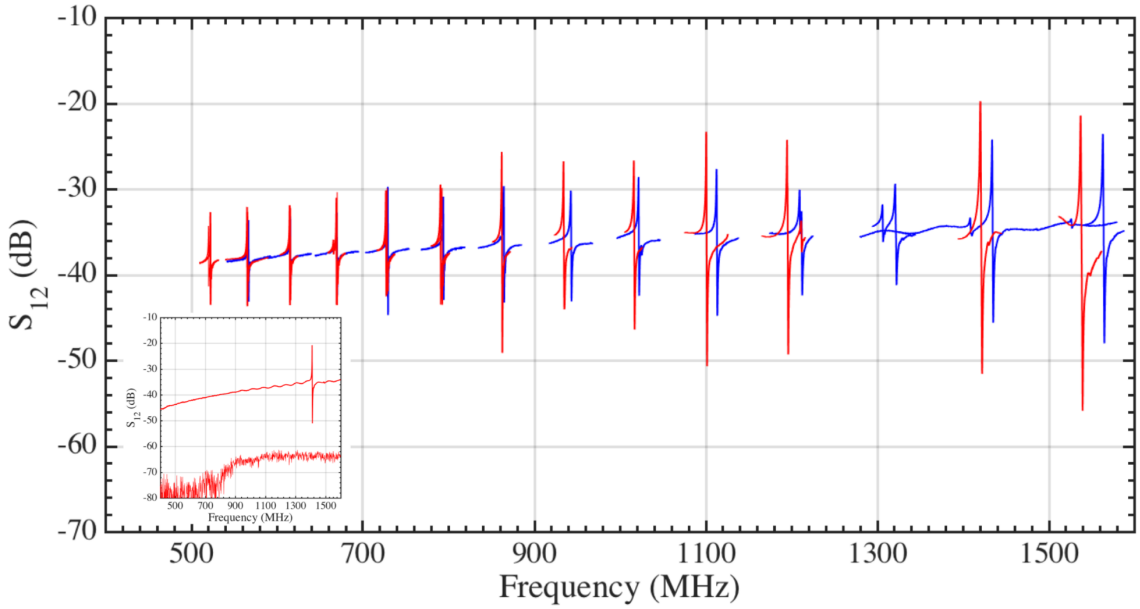

Figure 8. Narrow range frequency response of AlN (blue) and ScAlN (red) WE CMR released from high resistivity silicon. Resonances for ScAlN tend to improve in insertion loss and shift down in frequency. Inset) Wide range frequency response of a single ScAlN resonator and of probes on pads without an attached device.

To better quantify the improvements seen in the 12% Sc films, the BVD model was utilized to extract parameters. Utilizing the model, identification of the series resonance (f_s), the peak approaching 0 dB, and the parallel resonance (f_p), the peak approaching -100 dB, allows for a measurement of the k^2_{eff}, Eqn 3.

$$k_{eff}^2 = \frac{f_p^2 - f_s^2}{f_p^2} \sim \frac{d_{31}^2 E}{\epsilon} \quad (3)$$

This equation was applied for both the AlN (blue 'o') and ScAlN (red '^') devices and was plotted in Fig 9a. By linear least squares fitting of the data, a 36% improvement in k^2_{eff} could be measured. We note that refractive index, as measured using a Woolham ellipsometer, increased in the ScAlN films to 2.15 from AlN's measured value of 2.07. Further the acoustic velocity reduced in ScAlN compared to AlN by more than 1% suggesting that an increase in the d_{31} was the dominant factor in Eqn 3.

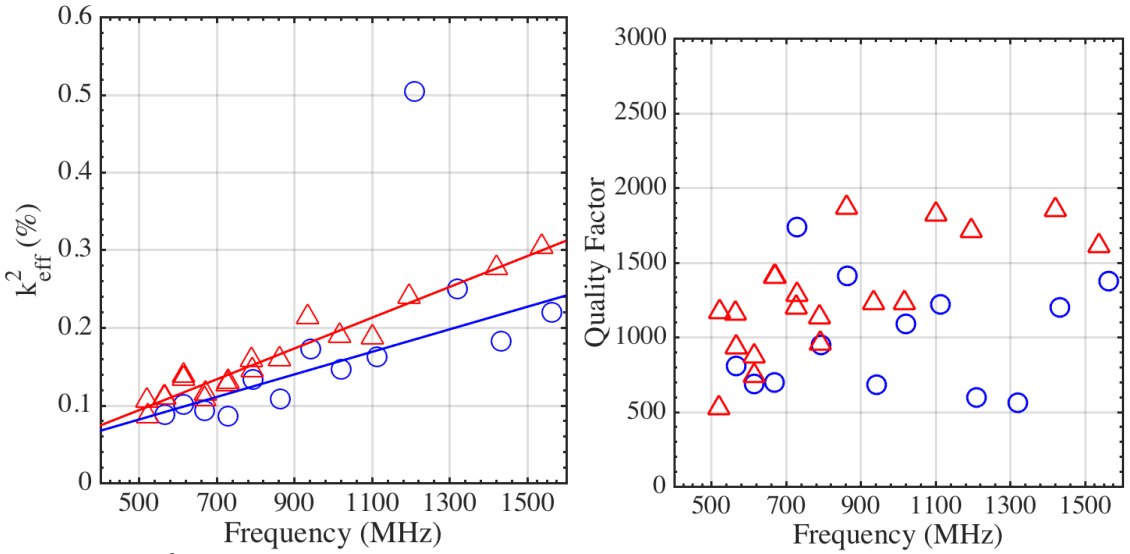

Figure 9. a) k^2_{eff} as a function of frequency for AlN (blue 'o') and ScAlN (red '^') with top electrode only, extracted from S_{21} series and parallel resonances. From the least squares linear fit of the slope we extract a 36% improvement. b) Unloaded quality factor of the series resonance for AlN (blue 'o') and ScAlN (red '^').

A second resonator parameter which quantifies the devices is the unloaded quality factor (Q_{ul}). The Q_{ul} of the f_s peak is determined by Eqn 4.

$$Q_{ul} = Q \frac{R_x}{100 + R_x} = \frac{f_s}{\Delta f_s} \frac{R_x}{100 + R_x} \quad (4)$$

Here R_x is the motional impedance at the series resonance, also seen as the insertion loss on resonance, and quality factor is defined classically as the resonance frequency divided by the -3 dB bandwidth. The Q_{ul} is influenced by all the potential energy loss mechanisms including electrical, electromechanical, and mechanical loss mechanisms. Since fabrication was identical for the two films, we assume that any significant change can be attributed to the piezoelectric films themselves. However, only a slight improvement for ScAlN Q_{ul}'s was noted which suggests both films were of good quality as noted by the rocking curves.

A standard metric for quantifying resonators is the figure of merit (FOM) as defined in Eqn 5.

$$FOM = k_{eff}^2 \, Q_{ul} \quad (5)$$

Comparison of the FOM shows a clear advantage of ScAlN over that of AlN, Fig 10.

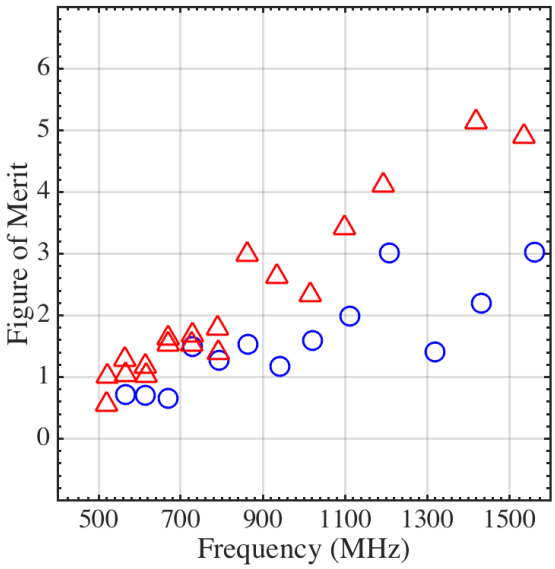

Figure 10. Figure of merit as a function of frequency for the WE CMRs for AlN (blue 'o') and ScAlN (red '^'). A clear improvement is observed for ScAlN.

Conclusions

This work has demonstrated a RF sputter process for developing WE contour mode top electrode resonators in $Sc_{0.12}Al_{0.88}N$ on high resistivity silicon. Measurements of the piezoelectric film demonstrated a rocking curve of 1.906° and resonators with a fundamental symmetric mode resonance from 500 MHz up to 1500 MHz. Utilizing the same sputter tool, AlN was also deposited on high resistivity silicon with a rocking curve of 2.248°. The same fabrication process yielded devices in the same frequency range. Comparison of the S_{12} response shows a marked improvement in both the series and parallel resonant peaks with a slight downward shift in acoustic velocity. From the BVD equivalent model, extracted k^2_{eff} and Q_{ul} values demonstrate modest improvements in the ScAlN film qualities. When combined, FOM suggests RF electrical gains can be found with Sc doping and utilization of both top and bottom electrodes would find increased value.

Establishing deposition conditions of AlN can prove difficult using a single sputter target and $Sc_{0.12}Al_{0.88}N$ seems to offer further challenges with grain inclusions in the piezoelectric film. This work required the use of four baffle wafers to decrease the inclusions down but significant more sputter science will be required to eliminate them. However, the advantages of utilizing increased Sc concentrations is demonstrating to be a high value added for CMR and RF filters.

Acknowledgments

This project was supported by the LDRD program at Sandia National Laboratories. Sandia National Laboratories is a multi-mission laboratory managed and operated by National Technology and Engineering Solutions of Sandia, LLC., a wholly owned subsidiary of Honeywell International, Inc., for the U.S. Department of Energy's National

Nuclear Security Administration under contract DE-NA-0003525. The authors acknowledge and thank the staff of Sandia's MESA fabrication facility and Dr. Steve Miller of H&M Analytical Services for XRD measurements.

References

1. C. D. Nordquist and R. H. Olsson, in *Wiley Encyclopedia of Electrical and Electronics Engineering* (John Wiley & Sons, Inc., 2014).
2. J. Kaitila, in *Ultrasonics Symposium , 2007. IEEE* (IEEE, New York, NY, 2007), pp. 120-129.
3. K.-y. Hashimoto and K.-Y. Hashimoto, *Surface acoustic wave devices in telecommunications*. (Springer, 2000).
4. G. Piazza, P. J. Stephanou and A. P. Pisano, Journal of Microelectromechanical Systems **15** (6) (2006).
5. K. Wojciechowski, C. D. Nordquist, B. Griffin, M. D. Henry and R. H. Olsson, 2013.
6. C. D. Nordquist, M. D. Henry, J. H. Nguyen, P. Clews, S. Lepkowski, A. Grine, C. W. Dyck and R. H. Olsson, presented at the Microwave Symposium (IMS), 2016 IEEE MTT-S International, 2016 (unpublished).
7. M. D. Henry, T. Young, A. E. Hollowell, M. Eichenfield and R. H. Olsson, in *Electronic Components and Technology Conference (ECTC) , 2015 IEEE 65th* (IEEE, San Diego, CA, 2015), pp. 1331-1337.
8. R. H. Olsson, J. G. Fleming, K. E. Wojciechowski, M. S. Baker and M. R. Tuck, presented at the Frequency Control Symposium, 2007 Joint with the 21st European Frequency and Time Forum. IEEE International, 2007 (unpublished).
9. G. Piazza, in *Resonant MEMS* (Wiley-VCH Verlag GmbH & Co. KGaA, 2015), pp. 147-172.
10. P. Muralt, in *Piezoelectric MEMS Resonators* (Springer, 2017), pp. 3-37.
11. A. Teshigahara, K.-y. Hashimoto and M. Akiyama, presented at the Ultrasonics Symposium (IUS), 2012 IEEE International, 2012 (unpublished).
12. M. Moreira, J. Bjurström, I. Katardjev and V. Yantchev, Vacuum **86** (1), 23-26 (2011).
13. S. Fichtner, T. Reimer, S. Chemnitz, F. Lofink and B. Wagner, APL Materials **3** (11), 116102 (2015).
14. F. Martin, P. Muralt, M.-A. Dubois and A. Pezous, Journal of Vacuum Science & Technology A: Vacuum, Surfaces, and Films **22** (2), 361-365 (2004).
15. D. Geiselman, Journal of the Less Common Metals **4** (4), 362-375 (1962).
16. V. Yantchev and I. Katardjiev, Journal of Micromechanics and Microengineering **23** (4), 043001 (2013).
17. J. Liang, H. Zhang, D. Zhang, X. Duan, H. Zhang and W. Pang, Journal of Micromechanics and Microengineering **25** (3), 035016 (2015).